American Journal of Physical Chemistry
2025, Vol. 14, No. 1, pp. 1-6
https://doi.org/10.11648/j.ajpc.20251401.11

Research Article

Influence of pH Variation on the Structural Properties of ZnS Nanocrystals Synthesized Via Low-Temperature Chemical Deposition

Bijoy Barman*

Department of Physics, Abhayapuri College, Abhayapuri, India

Abstract

The structural properties of nanomaterials play a crucial role in determining their performance in various applications. This study investigates the effect of pH variation on the structural properties of ZnS nanocrystals synthesized via low-temperature chemical deposition. ZnS nanoparticles were prepared in a polyvinyl alcohol (PVA) host matrix, with pH values ranging from 2.2 to 2.8. X-ray diffraction (XRD) analyses reveal that an increase in pH enhances crystallinity, resulting in narrower peaks and larger grain sizes. The average grain sizes of the films with varying pH values are found to range from 4.63 nm to 6.37 nm. The lattice constant evaluated using Nelson Reiley plot (N-R plot) ranges from 5.363 Å to 5.420 Å (pH 2.2-2.8), which slightly deviates from the standard 5.406 Å, suggesting compressive strain in the films, possibly due to sulfur deficiency. It was also observed that as pH decreases, there is an increase in microstrain and dislocation density probably due to lattice contraction. Results from the Williamson-Hall analysis confirm these trends, showing reductions in both average grain size and lattice strain at lower pH. These findings highlight the critical role of pH in controlling the structural characteristics of ZnS thin films, providing insights for optimizing ZnS properties for specific technological applications.

Keywords

ZnS Thin Films, Low Temperature, Structural Properties, pH Variation

1. Introduction

Zinc sulfide (ZnS) is a widely studied material known for its semiconducting properties and has gained significant attention because of its diverse applications in areas like optoelectronics, photocatalysis, and sensing [1-3]. The properties of ZnS, such as its optical and electronic characteristics, are highly dependent on its size, shape, and crystalline structure [4-6]. These structural properties, in turn, are influenced by the synthesis conditions, which include factors like temperature, precursor concentration, and pH Among these, pH is a critical parameter that can profoundly influence the processes of nucleation and growth during the synthesis of ZnS nanocrystals, thereby altering their structural and morphological features [7-9].

ZnS quantum dots can be prepared using a variety of approaches, including screen-based patterning, electrodeposition, vapor-phase condensation, sol-gel techniques, molecular beam epitaxy (MBE), and physical vapor deposition (PVD) and etc. [10-13]. However, these techniques often

*Corresponding author: kbbbijoy@gmail.com (Bijoy Barman)

Received: 27 January 2025; **Accepted:** 13 February 2025; **Published:** 24 February 2025

Copyright: © The Author(s), 2025. Published by Science Publishing Group. This is an **Open Access** article, distributed under the terms of the Creative Commons Attribution 4.0 License (http://creativecommons.org/licenses/by/4.0/), which permits unrestricted use, distribution and reproduction in any medium, provided the original work is properly cited.

require complex and expensive equipment, and issues such as thermal expansion mismatch between the film and the substrate can lead to the formation of microcracks. In contrast, low-temperature chemical deposition methods, like chemical bath deposition (CBD), offer a simpler and more economical approach to produce ZnS nanocrystals with controllable properties [14-16]. In these methods, the pH of the deposition solution is a key factor that governs the precipitation process of zinc and sulfide ions, thereby influencing the nucleation and growth of ZnS nanocrystals. Changes in pH can significantly affect the size, shape, and crystallinity of the resulting nanocrystals, which in turn modifies their optical, electronic, and mechanical properties [17]. Therefore, understanding how pH variation impacts the structural characteristics of ZnS nanocrystals is essential for optimizing their performance in various technological applications.

This study investigates how pH modification influences the structural characteristics of ZnS nanocrystals synthesized via low-temperature chemical deposition. By exploring the impact of pH on the synthesis of ZnS nanoparticles, this paper aims to provide insights into how pH influences the size, and crystallinity of ZnS nanocrystals.

2. Experimental

The ZnS nanoparticles examined in this study were synthesized within a polyvinyl alcohol (PVA) host matrix. A 2% PVA concentration was used for the bath solution to deposit all the ZnS films. To synthesize ZnS nanoparticles, 1.0 M $ZnCl_2$ solution was prepared in distilled water and was mixed with freshly prepared PVA host matrix. The solution was then stirred at 70°C until a clear solution was achieved. A solution of Na_2S in equimolar proportions was then slowly added drop by drop to the mixture while stirring continuously, until the solution became milky. The pH of the solution was adjusted by slowly adding the required amount of HNO_3 drop by drop. Four different pH value (2.2, 2.4, 2.6, 2.8) was prepared. The as prepared solutions were then casted over cleaned glass substrates to prepare thin films and dried under vaccum to remove the residual water. The structural properties of the films were analyzed using a Philips X'pert Pro X-ray diffractometer (XRD) and a Seifert X-ray diffractometer (303TT). Monochromatic CuKα radiation with a wavelength of 1.54056 Å was employed during the X-ray scan. The operating voltage of the X-ray tube was set to 40 kV – 30 mA for the X'pert Pro and 40 kV – 20 mA for the Seifert diffractometer.

3. Results and Discussions

Figure 1 displays the X-ray diffraction patterns of the ZnS films synthesized by varying the pH from 2.2 to 2.8. As observed in Figure 1, the crystalline quality of the films enhances with an increase in the pH of the solution. The XRD patterns in Figure 1 (a) show broad peaks at 2θ = 28.85°, 47.74°, and 56.83°, indicating the formation of nanostructures at pH = 2.2. Similarly, in Figure 1 (b), for pH = 2.4, broad peaks are observed at 2θ = 29.04°, 48.02°, and 56.72°. In Figure 1 (c), corresponding to pH = 2.6, the peaks are observed at 2θ = 29.19°, 48.18°, and 56.65°, while in Figure 1 (d), for pH = 2.8, the peaks appear at 2θ = 28.83°, 47.74°, and 56.52°.

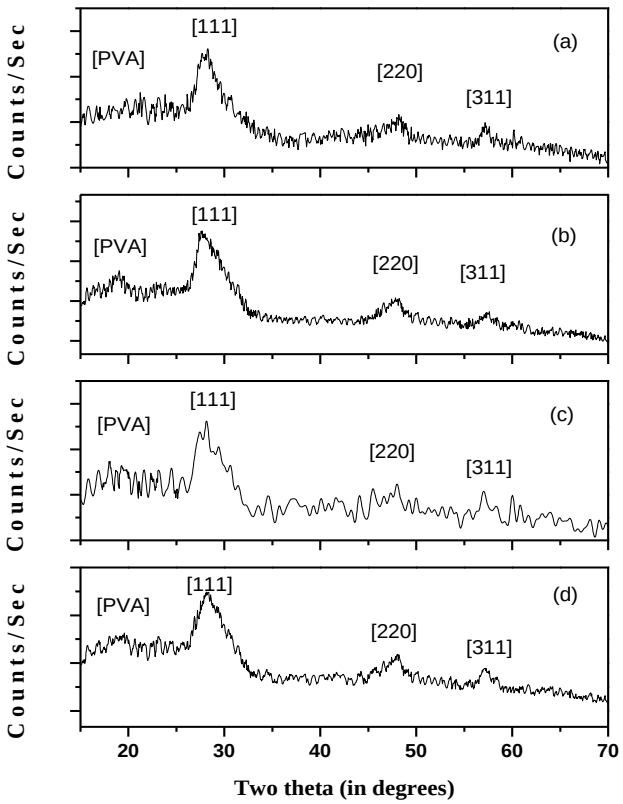

Figure 1. *X-ray diffraction patterns of nanocrystalline ZnS thin films as a function of pH variation (a) 2.2, (b) 2.4, (c) 2.6, (d) 2.8.*

The X-ray diffraction peaks observed for the planes (111), (220), and (311) of ZnS quantum dots incorporated in PVA polymer matrix indicate the presence of a cubic zinc blende structure (JCPDS card no. 5-0566). It is also evident that as the pH decreases, the diffraction peaks become broader and shift to higher angles, which is associated with decreasing the crystallite size [18-21]. The observed shift to a higher diffraction angle is attributed to lattice contraction, which occurs as a result of the increased surface-to-volume ratio at smaller crystallite sizes. [22]. Our study on the effect of pH variation by adding concentrated HNO_3 reveals that a pH of 2.2 is optimal for the growth of high-quality nanocrystalline films. At this pH, the ZnS samples predominantly exhibit the cubic ZnS phase [23, 24], and the peak positions align well with the values reported in the standard JCPDS card no. 5-0566.

Under acidic conditions, OH^- ions act as a catalyst in the growth of ZnS nanoparticles. These OH^- ions may enhance the ionization of Zn^{2+}, promoting a faster reaction with S^{2-} ions, which accelerates the formation of ZnS nuclei. As the number of nucleation sites increases, smaller particles tend to merge, leading to the formation of larger particles [25]. A diffraction peak at 2θ = 19.5° can be also observed in the XRD pattern that in all the spectra due to PVA. No undesired peaks corresponding to impurity phases were observed in the XRD pattern.

Table 1. *Calculated structural parameters of ZnS nanocrystalline thin films at various pH values.*

pH	[hkl] values	2θ (degree)	d value from XRD (Å)	F (θ)	a_{cal} (Å)	a corrected (Å)	Av. Internal stress (S) x 10^9 (N/m^2)	Av. Internal strain (ϵ) x 10^{-3}	Dislocation density (ρ x 10^{16}/ m^2)	Grain size (D) (nm)
	[111]	28.53	3.128	1.583	5.419					
2.2	[220]	48.05	1.893	0.567	5.355	5.363	1.721	8.41	8.89	4.63
	[311]	57.16	1.611	0.322	5.344					
	[111]	28.48	3.133	1.586	5.428					
2.4	[220]	47.97	1.896	0.569	5.364	5.390	1.608	7.88	8.01	4.99
	[311]	57.05	1.614	0.325	5.354					
	[111]	28.20	3.164	1.610	5.480					
2.6	[220]	47.82	1.902	0.574	5.379	5.408	1.373	6.54	7.70	5.69
	[311]	57.53	1.601	0.314	5.313					
	[111]	28.72	3.108	1.567	5.383					
2.8	[220]	48.12	1.891	0.564	5.348	5.420	1.220	4.39	5.87	6.37
	[311]	57.26	1.608	0.320	5.336					

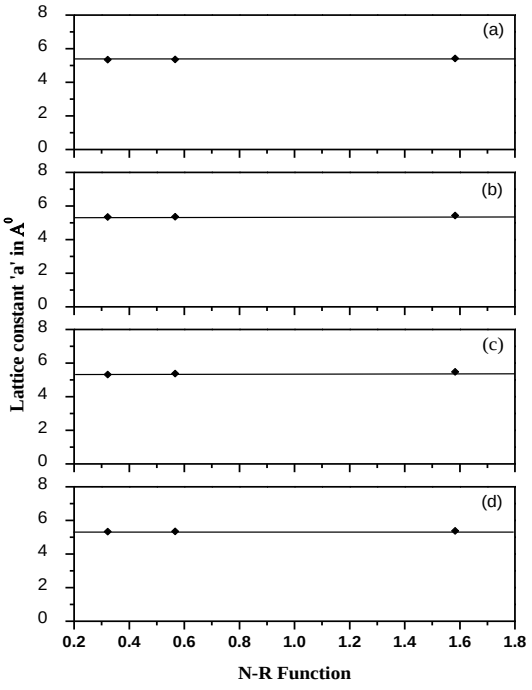

Figure 2. *Nelson-Riley plots for ZnS nanocrystalline films, prepared at different pH values (a) 2.2, (b) 2.4, (c) 2.6, (d) 2.8.*

The diffraction peak positions, along with their associated crystallographic planes, interplanar spacing, and the computed values for lattice constant, average stress, microstrain, and grain sizes, are summarized in Table 1. The lattice parameter 'a' for the cubic phase is calculated using Equation (1), as detailed below:

$$d_{hkl} = \frac{a}{\sqrt{h^2+k^2+l^2}} \quad (1)$$

The corrected values of the lattice constant are determined from the Nelson-Riley plots, as illustrated in Figure 2. The calculated lattice constant varies between 5.363 Å and 5.420 Å, showing a small deviation from the standard value of 5.406 Å (JCPDS card No. 5-0566). This variation indicates that the as-deposited films are subjected to compressive strain. A lower lattice constant could also indicate a sulfur deficiency in the films.

The average grain size 'D' was determined by analyzing the prominent peaks corresponding to the (111), (220), and (311) reflections using Equation (2), as follows:

$$D_{hkl} = \frac{K\lambda}{\beta_{2\theta}\ Cos\ \theta} \quad (2)$$

The average grain sizes of the films with varying pH values are found to range from 4.63 nm to 6.37 nm. It is observed that the grain size decreases as the pH value decreases, reaching its smallest size at pH 2.2. The presence of broad diffraction peaks further confirms the dominance of the nanocrystalline phase in these films.

We have also investigated the impact of pH on the average stress (S), strain (ε) and dislocation density (ρ) in different ZnS nanocrystalline thin films by the using equation (3), (4) and (5) respectively.

$$S = \frac{Y}{2\sigma}\left[\frac{(a_o - a)}{a_o}\right] \quad (3)$$

$$\varepsilon = \left[\frac{(a_o - a)}{a_o}\right] \quad (4)$$

$$\epsilon_{hkl} = \frac{\beta_{2\theta}\ Cot\ \theta}{4} \quad (5)$$

Here, a_o and a (from the N-R plot) represent the lattice parameters of the film samples and bulk samples, respectively. 'Y' denotes Young's modulus, and 'σ' refers to Poisson's ratio of the samples. $\beta_{2\theta}$ is the full width at half maximum (FWHM) of the peaks, and θ is the Bragg angle. It is also observed that as the pH of the nanoparticle solution decreases, both microstrain and dislocation density tend to increase. Figure 3 Illustrates the variation of lattice constant, average stress, average strain, dislocation density, and average grain size across different pH levels in ZnS nanocrystalline thin films.

The grain size and the average strain in the as prepared ZnS films are also calculated by Williamson and Hall method using equation (6) as follows:

$$\beta = \frac{\lambda}{D\cos\theta} + 4\varepsilon\tan\theta \quad (6)$$

Here, θ represents the Bragg angle of the XRD peak, and λ is the wavelength of the X-ray used, which is CuKα radiation (λ=1.542 Å), 'D' denotes the effective particle size, and ϵ refers to the effective strain. To obtain the corrected values, the full width at half maximum (FWHM) of the fitted diffraction peak was determined by subtracting the instrumental broadening from the experimental integral width. A plot of $\frac{\beta\ \cos\theta}{\lambda}$ versus $\frac{2\ \sin\theta}{\lambda}$ was then constructed for each film, as shown in Figure 4.

The average grain size (D) was determined from the inverse of the intercept on the y-axis, while the average strain (ϵ) was calculated from the slope of the linear plots. The calculated values for the average grain size (D) and average strain (ϵ) for different films are presented in Table 2 and illustrated in Figure 5. The results derived from the W-H plot also indicate a decrease in both the average grain size and strain as the pH is reduced.

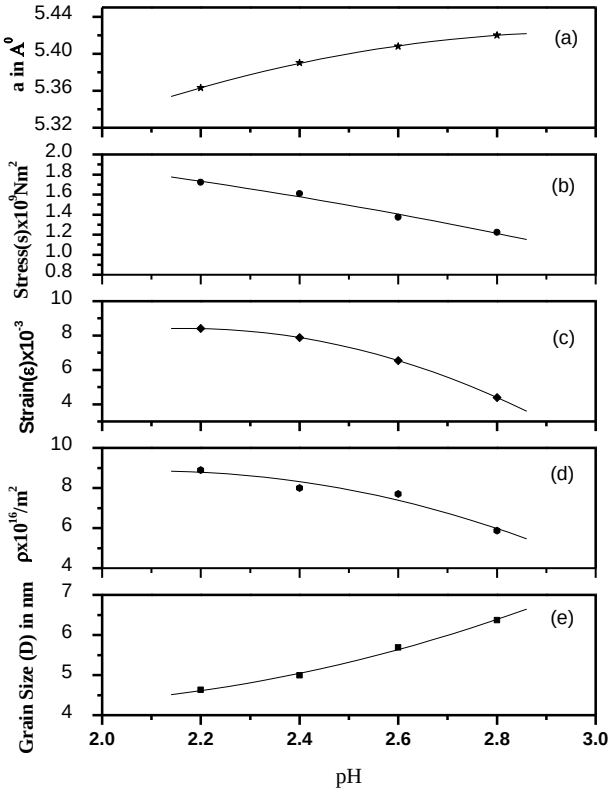

Figure 3. *Variation of (a) Lattice constant, (b) Average stress, (c) Average strain, (d) Dislocation density and (e) Average grain size with different pH value of ZnS nancrystalline thin films.*

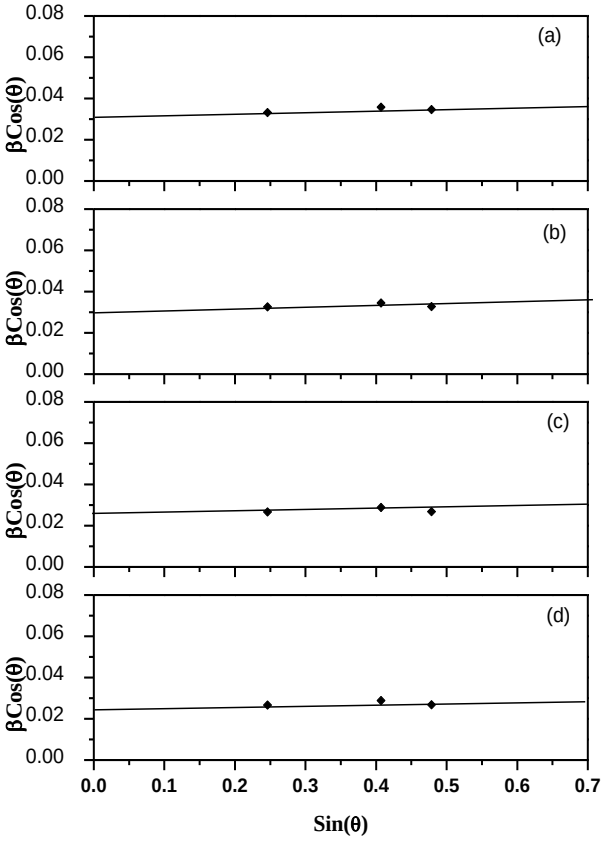

Figure 4. *W-H plots for ZnS nanocrystalline thin films for different pH value (a) 2.2, (b) 2.4, (c) 2.6, (d) 2.8.*

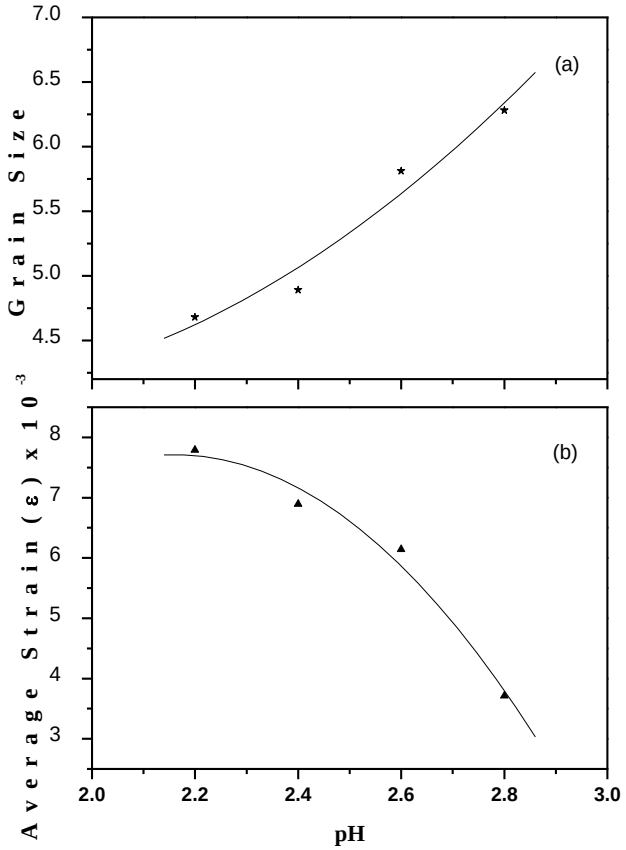

Figure 5. *Change in (a) average grain size and (b) average strain from the W-H plot for ZnS nanocrystalline films at varying pH values.*

Table 2. *Estimated values of grain size and lattice strain evaluated from the W-H plots for ZnS nanocrystalline thin films for different pH value.*

Parameters	Different pH of ZnS thin films			
	2.2	2.4	2.6	2.8
Grain size D (in nm)	4.68	4.89	5.81	6.28
Average lattice strain (ε)	7.97 x 10^{-3}	6.89 x 10^{-3}	6.14 x 10^{-3}	3.71 x 10^{-3}

4. Conclusion

In conclusion, the study demonstrates that pH variation significantly impacts the structural properties of ZnS nanocrystalline thin films. X-ray diffraction (XRD) analysis indicates that higher pH levels improve crystallinity, producing narrower peaks and larger grain sizes, which range from 4.63 nm to 6.37 nm across the samples. The lattice constant, determined using the Nelson-Riley (N-R) plot, spans from 5.363 Å to 5.420 Å (for pH 2.2 to 2.8), slightly below the standard 5.406 Å, suggesting compressive strain likely due to sulfur deficiency. Additionally, as pH decreases, microstrain and dislocation density increase, likely caused by lattice contraction. Williamson-Hall analysis supports these findings, revealing decreases in both average grain size and lattice strain at lower pH levels. Optimal nanocrystalline film growth, with favorable cubic ZnS phase formation, was observed at pH 2.2. These findings contribute to a deeper understanding of pH effects in ZnS synthesis, providing valuable insights for synthesizing ZnS nanocrystals for enhanced performance in optoelectronic, catalytic, and sensor applications. Expanding the study to a broader pH range could provide deeper insights into its effects on ZnS nanocrystals beyond the investigated values. *Exploring different stabilizing agents or deposition conditions may further enhance crystallinity and structural properties. Additionally, advanced characterization techniques such as high-resolution transmission electron microscopy (HRTEM) or Raman spectroscopy could offer a more detailed analysis of defects, strain, and phase stability. These investigations would contribute to a comprehensive understanding of pH-dependent modifications in ZnS nanocrystals, facilitating their applications in optoelectronic and sensing technologies.*

Abbreviations

XRD	X-ray Diffraction
N-R Plot	Nelson Reily Plot
W-H Plot	Williamson Hall Plot
ZnS	Zinc Sulfide
MBE	Molecular Beam Epitaxy
PVD	Physical Vapour Deposition
CBD	Chemical Bath Deposition
PVA	Polyvinyal Alcohol
FWHM	Full Width at Half Maximum

Acknowledgments

The authors are thankful to Department of Physics, Department of Nanotechnology and CIF, IIT Guwahati and Department of Instrumentation and USIC for providing XRD facilities.

Author Contributions

Bijoy Barman is the sole author. The author read and approved the final manuscript.

Conflicts of Interest

The author declares no conflicts of interest.

References

[1] YM. Suhail, Structural and optical properties of ZnS, PbS, Zn1-xPbxS, ZnxPb1-xS and PbZnxS1-x thin films, Indian Journal of Pure & Applied Physics. 50, 380-386 (2012). https://www.researchgate.net/publication/298417440

[2] M. Temiz, and S. Çelik, Influence of growth temperature on the structural and optical characteristics of PbZnS thin films, Chalcogenide Letters, 21, 867-872 (2024). https://doi.org/10.15251/CL.2024.2111.867

[3] B. Barman, and K. C. Sarma, Low temperature chemical synthesis of ZnS, Mn doped ZnS nanosized particles: Their structural, morphological and photophysical properties, Solid State Sciences. 109, 106404 (2020). https://doi.org/10.1016/j.solidstatesciences.2020.106404

[4] B. Barman, and K. C. Sarma, Structural characterization of PVA capped ZnS nanostructured thin films, Indian J Phys. 86, 703-707 (2012). https://doi.org/10.1007/s12648-012-0116-0

[5] Z. Jiang, A. Hoffmann, and A. Schleife, Influence of temperature, doping, and amorphization on the electronic structure and magnetic damping of iron Phys. Rev. B., 109, 235247 (2024). https://doi.org/10.1103/PhysRevB.109.235147

[6] B. D. Cullity, Elements of X-ray Diffraction, Addison-Wesley Publishing Company, Inc. 187 (1978).

[7] Göde, F., Annealing temperature effect on the structural, optical and electrical properties of ZnS thin films, Physica B: Condensed Matter. 406, 1653-1659 (2011). https://doi.org/10.1016/j.physb.2010.12.033

[8] B. Barman and K. C. Sarma, Luminescence Properties of ZnS Quantum Dots Embedded in Polymer Matrix, Chalcogenide Letters. 8, 171-176 (2011).

[9] T. Sinha, D. Lilhare, A. Khare, Effects of Various Parameters on Structural and Optical Properties of CBD-Grown ZnS Thin Films: A Review, Journal of Electronic Materials. 47(2), 1730-1751 (2018).

[10] H. E. Ruda, Wide gap II-VI Compound for optoelectronic applications, Chapman and Hall, London (1992).

[11] S. Kar S. Biswas, S. Chaudhuri and P M G Nambissan, Substitution-induced structural transformation in Mn-doped ZnS nanorods studied by positron annihilation spectroscopy, Nanotechnology. 18, 225606 (2007). https://doi.org/10.1088/0957-4484/18/22/225606

[12] P. Vasa, P. Ayyub and B. P. Sing, Fast and reversible excited state absorption in II-VI-based nanocomposite thin films, Appl. Phys. Lett. 87, 063104 (2005). https://doi.org/10.1063/1.2007871

[13] S, Chanda, M. Debbarma, D, Ghosh, B. Debnath and S. Chattopadhyaya, First-Principles Investigation of Structural, Elastic, Electronic, and Optical Properties of Cd1−x−yZnxHgyS Quaternary Alloys, Journal of Electronic Materials. 8, 4705-4726 (2021). https://doi.org/10.1007/s11664-021-08986-6

[14] A. Z. Arsad, A. W. M. Zuhdi, S. F. Abdullah, C. F. Chau, A. Ghazali, I. Ahmad, and W. S. W. Abdullah, Effect of Chemical Bath Deposition Variables on the Properties of Zinc Sulfide Thin Films: A Review, Molecules. 28, 2780 (2023). https://doi.org/10.3390/molecules28062780

[15] A. Barman, and K. C. Sarma, Synthesis and optical properties of ZnS nanoparticles in PVA matrix, Optoelectronics and Advanced Materials - Rapid Communications. 4, 1594-1597 (2010).

[16] S. Kumar, S. Bakshi, S. Chaudhary, J. Kaur, A. P. Agrawal, and S. Rani, Heat Post-Treatment Effect on Optical and Electrical Properties of ZnS Thin Films, Biointerface Research in Applied Chemistry. 14, 1-9 (2024). https://doi.org/10.33263/BRIAC144.100

[17] B. Siahmardan, V. Soleimanian, and M. G. Varnamkhasti, Effect of size and shape of crystallites on the optical properties of nanostructured ZnS films, Materials Science in Semiconductor Processing. 71, 76-83 (2017). https://doi.org/10.1016/j.mssp.2017.06.041

[18] A. Nazim, and B. Parveen, Synthesis of Zn metal contents-dependent ultra-wide-band gap ZnS nanoparticles, Applied Physics A. 129, 808 (2023). https://doi.org/10.1007/s00339-023-07069-z

[19] J. Barman, and F. Sultana, Synthesis of mix Zinc oxide and Cadmium sulphide Nanoparticles, Optoelectronic and antimicrobial activity and application in Water Treatment, IOSR Journal of Applied Physics. 8, 46-51 (2016). https://doi.org/10.9790/4861-0801044651

[20] J. Angel Mary Greena, K. Karuppasamy, R. Antony, X. Sahaya Shajan and S. Kumaresan, Structural, Thermal and Spectroscopic Studies on Zinc Doped Strontium Formate Dihydrate Crystals, IOSR Journal of Applied Physics. 1, 25-28 (2012). https://doi.org/10.9790/4861-0142528

[21] B. Barman, P. K. Mochahari, and K. C. Sarma, Optical Studies on Some Aspects of Polyvinyl Alcohol Composite Zns Nanocrystalline Thin Films, AIP Conference Proceedings. 1391, 116-118 (2011).

[22] K. K. Nanda, S. N. Sarangi, and S. N. Sahu, CdS Nanocrystalline films: Composition, surface, crystalline size, structural and optical absorption studies. Nanostructured materials 10 1401-1410 (1998).

[23] R. B. Kale and C. D. Lokhande, Band gap shift, structural characterization and phase transformation of CdSe thin films from nanocrystalline cubic to nanorod hexagonal on air annealing, Semiconductor Science and Technology. 20, 201 (2005). https://doi.org/10.1088/0268-1242/20/1/001

[24] L. Wang, L. Cao, G. Su, W. Liu, C. Xia, and H Zhou, reparation and characterization of water-soluble ZnSe: Cu/ZnS core/shell quantum dots, Applied Surface Science. 280, 673-678 (2013). https://doi.org/10.1016/j.apsusc.2013.04.174

[25] A. Goudarzi, G. M. Aval, R. Sahraei, and H. Ahmadpoor, Ammonia-free chemical bath deposition of nanocrystalline ZnS thin film buffer layer for solar cells, Thin Solid Films, 516, 4953-4957 (2008). https://doi.org/10.1016/j.tsf.2007.09.051